

# Gemini Surfactants at the Air/Water Interface: A Fully Atomistic Molecular Dynamics Study<sup>†</sup>

Ekta Khurana,\* Steven O. Nielsen,<sup>‡</sup> and Michael L. Klein

Center for Molecular Modeling and Department of Chemistry, University of Pennsylvania, Philadelphia, Pennsylvania 19104-6323

Received: May 30, 2006; In Final Form: August 3, 2006

Gemini surfactants typically consist of two single-chain surfactants chemically linked by a spacer molecule. We report herein the results of fully atomistic molecular dynamics (MD) simulations of a series of Gemini surfactants:  $C_3H_7\text{-}\alpha,\omega\text{-bis}(C_{12}H_{25}N^+(\text{CH}_3)_2Cl^-)$ , at the air/water interface with  $s = 3, 4, 6, 12, 14,$  and  $16$ , at values of the initial surface area per surfactant  $A_S = 70 \text{ \AA}^2, 77 \text{ \AA}^2, 95 \text{ \AA}^2, 151 \text{ \AA}^2, 133 \text{ \AA}^2,$  and  $103 \text{ \AA}^2$ , respectively. The  $A_S$  values employed were obtained from surface tension and neutron reflection experiments at the respective cmc of each surfactant. The Gemini surfactant corresponding to  $s = 3$  was also simulated at  $A_S = 105 \text{ \AA}^2$ , which is the experimentally derived value of surface area per surfactant at 1/10th of cmc. Only the surfactants with  $s = 12$  and  $14$  and the surfactant with  $s = 3$  at  $A_S = 105 \text{ \AA}^2$  gave a stable monolayer at the air/water interface. In other cases, we observe movement of some surfactant molecules from the air/water interface into the aqueous phase, resulting in a stable primary monolayer of surfactants at the air/water interface and a small concentration of surfactant molecules below it. The latter form aggregates, with their hydrophobic chains in the core. The density profiles along the normal to the interface are compared with the ones obtained from neutron reflection experiments. The MD simulations confirm the bending of the spacer toward the hydrophobic chains as the spacer length is increased and the spacer becomes more hydrophobic. The simulations have helped to shed light on the low-resolution picture which emerges from experimental analyses.

## Introduction

Gemini surfactants are formed from two monomeric surfactants that are linked by a spacer group close to the headgroups. The current interest arises primarily from their lower critical micelle concentration (cmc), greater surface tension lowering at the air/water interface, and the high viscosity of aqueous solutions of Gemini surfactants with short spacers at relatively low surfactant concentration<sup>1,2</sup> than achievable with corresponding monomeric surfactants. The behavior of Gemini surfactants at interfaces and in aqueous solution has been discussed in the review by Zana.<sup>3</sup> In this article, we focus on Gemini surfactants,  $[C_{12}H_{25}N(\text{CH}_3)_2-(\text{CH}_2)_s-N(\text{CH}_3)_2C_{12}H_{25}]_2$  (where I is the counterion), which are commonly referred to as  $m-s-m, 2I^-$ . We will employ the same notation in this article, namely, 12-3-12, 12-4-12, and so on. Such surfactants, which contain a polymethylene spacer, have been thoroughly investigated.<sup>4</sup>

The Gemini surfactants at the air/water interface have been studied by surface tension<sup>5</sup> and neutron reflection experiments.<sup>6,7</sup> The various models used to understand them have been discussed in detail by Diamant and Andelman in *Gemini Surfactants: Interfacial and Solution-Phase Behavior*.<sup>8</sup> The behavior is different from that of regular surfactants in many respects, which poses challenges to their complete understanding. The important puzzles raised by Gemini surfactants are exhibited in their surface activity, micellization point, aggregate shape, phase behavior, and dynamics.<sup>9</sup> However, our focus here in this study is the effect of spacer length,  $s$ , on the behavior of

the 12- $s$ -12 series at the air/water interface using classical MD simulations and fully atomistic force fields.

The surface tension of  $C_3H_7\text{-}\alpha,\omega\text{-bis}(C_{12}H_{25}N^+(\text{CH}_3)_2Br^-)$  with  $s = 3, 4, 6, 8, 10, 12, 14,$  and  $16$  was measured by Alami et al. as a function of the surfactant concentration.<sup>5</sup> They observed that the surface area per molecule,  $A_S$ , goes through a maximum for  $s = 10, 12$ . The reason for the non-monotonic increase in  $A_S$  with increasing spacer length was postulated to arise from the bending of the spacer at  $s \geq 10-12$ . Above this spacer length, the spacer is too hydrophobic to remain in contact with water and moves to the air side of the interface. The non-monotonic variation of  $A_S$  corresponds to the non-monotonic variation of the cmc upon increasing spacer length. The bending of the Gemini surfactant linkers has been confirmed by simple models<sup>10-12</sup> and neutron reflection experiments.<sup>6,7</sup> The surface excess concentration and  $A_S$  were calculated by Alami et al. using the Gibbs equation

$$(2.303nRT)\Gamma = -(d\gamma/d \log C)_T \quad (1)$$

with the equation

$$A_S = (N_A\Gamma)^{-1} \quad (2)$$

Here,  $\Gamma$  is the surface excess concentration,  $\gamma$  is the surface tension,  $R$  is the gas constant,  $T$  is the temperature,  $C$  is the surfactant concentration (in moles of surfactant per liter),  $n = 2$  (for univalent ionic surfactant) or  $n = 3$  (for divalent ionic surfactant), and  $N_A$  is Avogadro's number. The nature of ionic dimeric surfactants in aqueous solutions at concentrations below the cmc has been discussed by many authors. The state of the

<sup>†</sup> Part of the special issue "Charles M. Knobler Festschrift".

<sup>‡</sup> Present address: Department of Chemistry, University of Texas at Dallas, P.O. Box 830688, Richardson, TX 75083-0688.

surfactant governs the value of  $n$  that should be used in calculating  $A_S$ . The different values of  $n$  used have been discussed in the review by Zana.<sup>3</sup> It has been argued that for bis(quarternary ammonium) surfactants one counterion is associated with one ionic head, and therefore,  $n = 2$  should be used in calculating  $\Gamma$ .<sup>13,14</sup> However, the value of  $n$  used has no bearing on the non-monotonic increase in  $A_S$  upon increasing the value of  $s$ . Neutron reflection measurements by Li et al.<sup>6,7</sup> showed that the value of  $n$  used should be 2 for the systems being studied here, as the values of  $A_S$  obtained from neutron reflection experiments then agree with the ones obtained from surface tension measurements. Besides the value of  $A_S$ , the neutron reflection experiments by Li et al. have also been used to study the structure of monolayers of Gemini surfactants at the air/water interface.<sup>7</sup> They found that a low-concentration single layer of surfactants forms below the main layer at an approximate distance of 15–20 Å from the center of the headgroup distribution (normal to the interface). The area per molecule in this secondary layer did not seem to show any particular concentration dependence. It was proposed that this sublayer could be a manifestation of pre-micellar aggregation. The aim of the MD study conducted here was to throw more light on the surfactant behavior as discussed above and thereby obtain a more detailed picture of the monolayers. To our knowledge, this is the first attempt to study the behavior of these surfactants at the air/water interface by fully atomistic MD simulations.

### Simulation Details

Different choices can be made for setting up the system for the MD study of monolayers at air/water interfaces. It is possible to simulate a single monolayer in contact with the aqueous solution and confine the solution by placing a hard wall below the interface.<sup>15</sup> This requires a relatively large bath of water molecules for a given number of surfactants to avoid artifacts due to the long-range structuring of water by the wall.<sup>16</sup> A commonly used practice is to use a thick slab of water with the top and bottom covered with surfactant monolayers, with the thickness of the slab being large enough so that the two monolayers have practically no influence on each other.<sup>17</sup> Along these lines, all the systems studied here consisted of a slab of water with vacuum at either end resulting in two vacuum/water interfaces (also referred to as air/water interfaces in this article). Each system consisted of two monolayers of surfactant molecules at the two vacuum/water interfaces with 64 surfactant molecules in each layer. The water slab used was about 75 Å thick, and the cell size in the  $z$  dimension (normal to the interface) was 223 Å. In principle, a two-dimensional Ewald summation method such as that developed by Hautman and Klein<sup>18</sup> could be employed for handling the long-range electrostatic interactions. However, an efficient use of this method requires that the dimension in the nonperiodic direction be much smaller than the periodic directions, and this criterion is not met by the system sizes being studied here. Hence, periodic boundary conditions were employed in three dimensions, and long-range, electrostatic forces were taken into account using the particle mesh Ewald approach with a real-space cutoff of 12 Å.<sup>19,20</sup>

As mentioned above, the surfactants studied here are referred to as  $m-s-m$ , where  $m$  denotes the length of the hydrophobic chain and  $s$  denotes the length of the spacer, respectively. Six fully atomistic MD simulations were performed for 12–3–12 (system Ia), 12–4–12 (system II), 12–6–12 (system III), 12–12–12 (system IV), 12–14–12 (system V), and 12–16–12

**TABLE 1: Surface Area Per Gemini Surfactant,<sup>a</sup>  $A_S/\text{Å}^2$**

spacer length, $s$ for 12- $s$ -12 Gemini surfactants	neutron reflectivity area <sup>7</sup>	surface tension, area for $n = 2$ <sup>5</sup>	initial values for MD simulations
3	67 ± 3	70	70
4	85 ± 2	77	77
6	92 ± 3	95	95
12	134 ± 3	150	151
14	NA	133	133
16	NA	102	103

<sup>a</sup> Shown in the columns are values for the air/water interface, as measured from neutron reflection experiments and surface tension experiments at the respective cmc. The third column shows the initial surface area per molecule values used in the MD simulations. NA indicates that data are not available.

(system VI), respectively, at  $A_S$  values measured at cmc by previous experimental studies. Table 1 shows the  $A_S$  values measured using neutron reflection experiments (for the primary monolayer)<sup>7</sup> and measured using surface tension experiments<sup>5</sup> at cmc, and the initial surface area per molecule used in our MD simulations.

If the value of  $n$  used in the Gibbs equation is 3 instead of 2, for 12–3–12, the  $A_S$  value as measured from the surface tension measurement is 105 Å<sup>2</sup>.<sup>5</sup> Also, coincidentally,  $A_S$  is 105 Å<sup>2</sup> at one-tenth of the cmc as measured by neutron reflection experiments.<sup>7</sup> We performed an additional simulation of the surfactant 12–3–12 at an initial surface area per molecule corresponding to 105 Å<sup>2</sup>, which is referred to as system Ib.

To neutralize the positive charge on the surfactant molecules, 256 chloride ions were added randomly in the water of each system. The system sizes varied from 43 343 atoms to 85 967 atoms. The water molecules were described using the TIP3P model.<sup>21</sup> MD simulations were carried out using the program *NAMD* version 2.5b1<sup>22</sup> and the CHARMM force field.<sup>23</sup> The parameters and charges for the headgroup used were based on the CHARMM force field for tetramethylammonium groups. The *NVT* ensemble was used for all the simulations. Langevin dynamics was used to control the temperature at 300 K. A time step of 2 fs was used. Nonbonded interactions were calculated every time step, and full electrostatic interactions were calculated every two time steps. Bonds between hydrogen atoms and heavy atoms were constrained to their equilibrium value by means of the SHAKE/RATTLE algorithm.<sup>24,25</sup>

The length of the MD trajectory was ~17 ns for 12–4–12 (system II) and ~15 ns for 12–16–12 (system VI). The simulation time for all the other MD runs was ~10 ns.

The instantaneous surface tension was computed as follows:

$$\gamma_{\text{inst}} = \left(\frac{L_z}{2}\right) \left[ P_{zz} - \left(\frac{P_{xx} + P_{yy}}{2}\right) \right] \quad (3)$$

Here,  $L_z$  is the box size in the  $z$  direction (the direction normal to the air/water interface) and  $P_{ij}$  is the  $ij$  component of the pressure tensor. The first factor of  $1/2$  is to account for the two interfaces in the simulation box.

Simulation of pure vacuum/water interface was performed to calculate the air/water surface tension. As discussed for the systems above, the box consisted of two vacuum/water interfaces. The box dimensions were 40 Å × 40 Å × 120 Å. The vacuum/water interfaces were in the  $z$  direction. The thickness of water layer in the  $z$  direction was 40 Å, and the MD trajectory lasted ~9 ns.

### Results and Discussion

The average surface tension of the air/water interface using TIP3P water model and the particle mesh Ewald approach for

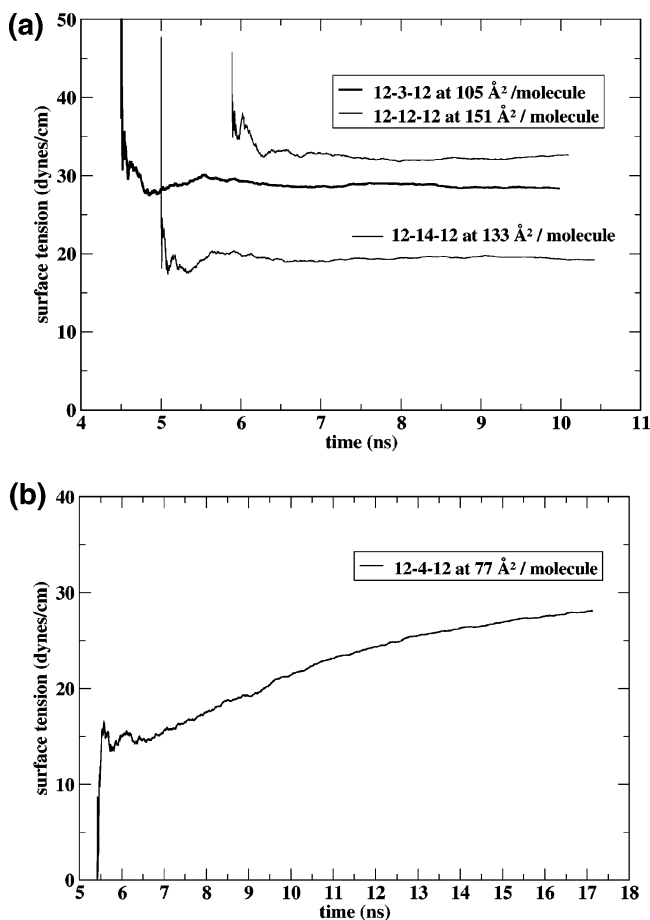


**Figure 1.** Cumulative average of the surface tension vs simulation time. Panel a is for the systems where a stable monolayer exists at the air/water interface throughout the simulation. Panel b is for system II where the surfactants molecules move from the air/water interface into the water phase and exhibit aggregate formation below the interface (also see Figure 3).

electrostatics with a real-space cutoff of 12 Å was calculated to be 52.75 dynes/cm. The surface tension was computed by averaging  $\gamma_{\text{inst}}$  over the length of the MD trajectory. The surface tension value calculated in our simulation agrees with the value of 52.7 dynes/cm calculated using the Ewald summation method for electrostatics by Feller et al.<sup>26</sup> The experimental value for the surface tension of water is 72.8 dynes/cm. Figure 1 shows the average surface tension versus simulation time for the different systems. The surface tension values plotted are the values of the cumulative average computed by averaging  $\gamma_{\text{inst}}$  over the length of the trajectory. The instantaneous surface tension was calculated from the pressure tensor every picosecond, using eq 3 as explained in the Simulation Details section. The exact values of the surface tension as shown in Figure 1 can be misleading. The reason is as follows. We have calculated the surface tension of a pure air/water interface with TIP3P water model and found that it is much lower than the experimental value. The lowering of the surface tension at the air/water interface by the surfactant molecules as described by the CHARMM force field might also not be equal to the lowering of surface tension by the surfactant molecules as measured experimentally. Accordingly, we focus more on the change in surface tension with time for the various simulations rather than the absolute value of the surface tension.

Figure 2 shows the number density profiles of water, ions, and different fragments of the surfactant molecules: headgroups (H), chains (C), and spacers (S); along the normal to the air/

water interface. The density profiles of chains, headgroups, and spacers for 12-3-12, 12-4-12, and 12-12-12 at  $A_S = 105$  Å<sup>2</sup>, 77 Å<sup>2</sup>, and 151 Å<sup>2</sup>, respectively, can be fit to Gaussians of the form

$$\rho(z) = \left( \frac{2A}{\sigma A_S \sqrt{\pi}} \right) \exp\left( \frac{-4(z - \mu)^2}{\sigma^2} \right) \quad (4)$$

Here,  $z$  is the distance along the normal to the interface,  $\rho(z)$  is the number density along  $z$ ,  $A$  is a constant,  $\sigma$  is the full width at  $1/e$  of the height,  $A_S$  is the initial surface area per surfactant, and  $\mu$  is the value of  $z$  at the center of distribution. Slight asymmetry in the density profiles introduces a small bias in fitting the curves to a single Gaussian. The values of this bias were estimated for different curves and were found to be very small.

The distributions obtained from the MD simulations are compared with analogous data obtained from fitting to the neutron reflection measurements<sup>7</sup> in Table 2. There, we report  $\sigma$  values obtained for C, H, and S from the simulations, while the  $\sigma$  values were assumed to be identical for the different fragments of the surfactant molecule while fitting neutron reflection data to the Gaussian functional form. It can be seen in Table 2 that the  $\sigma$  values obtained from our simulations are slightly lower than the experimental values.  $\delta_{\text{CH}}$  and  $\delta_{\text{SH}}$  denote the distance between the centers of distributions of chains and headgroups, and spacer and headgroups, respectively. The values shown are the average values calculated for two monolayers at the two air/water interfaces in each system. If  $\delta_{\text{CH}}$  stands for center of distribution for chains minus center of distribution for headgroups, it has opposite signs for the density profiles along the negative  $z$  axis and the positive  $z$  axis in Figure 2. However, a negative sign is used for easy comparison with the parameters obtained experimentally. The same discussion holds for  $\delta_{\text{SH}}$  values. We observe a higher  $\delta_{\text{SH}}$  value for 12-12-12 compared to 12-3-12 and 12-4-12. This shows that, as the spacer becomes more hydrophobic and longer, it bends toward the chains, and the density profiles of spacers move toward the density profiles of chains from those of the headgroups.

Figure 2a shows the density profiles for 12-3-12 at  $A_S = 70$  Å<sup>2</sup> (system Ia), computed over the last 2 ns of the simulation. We observe movement of some surfactant molecules from the interface into the aqueous phase and their self-assembly to give a spherical micellar structure. Even at the end of 10 ns, we observe that the system is not yet equilibrated. Similar behavior was observed for 12-4-12 (system II), and that system was run for a longer time to allow for further equilibration of the system. The large system sizes lead to extensive computational time and thus did not allow us to run all the systems for long trajectories. As seen from the density profiles in Figure 2a, the ions are associated with the headgroups, and the density profiles of the spacer chains also lie close to the profiles for the headgroups.

Figure 1a shows the average surface tension versus simulation time for the simulation of 12-3-12 at  $A_S = 105$  Å<sup>2</sup> (system Ib) calculated for about last 5 ns of the simulation. The average value of surface tension at the end of 10 ns was calculated to be 28.3 dynes/cm. The surface tension of this system corresponding to  $A_S = 105$  Å<sup>2</sup> in the primary layer is not available via neutron reflection experiments. However, as discussed in the Simulation Details, this corresponds to the surface area per molecule at cmc, if the value of  $n$  used in the Gibbs equation for calculating surface area from surface tension measurements is 3 instead of 2. The value of surface tension measured

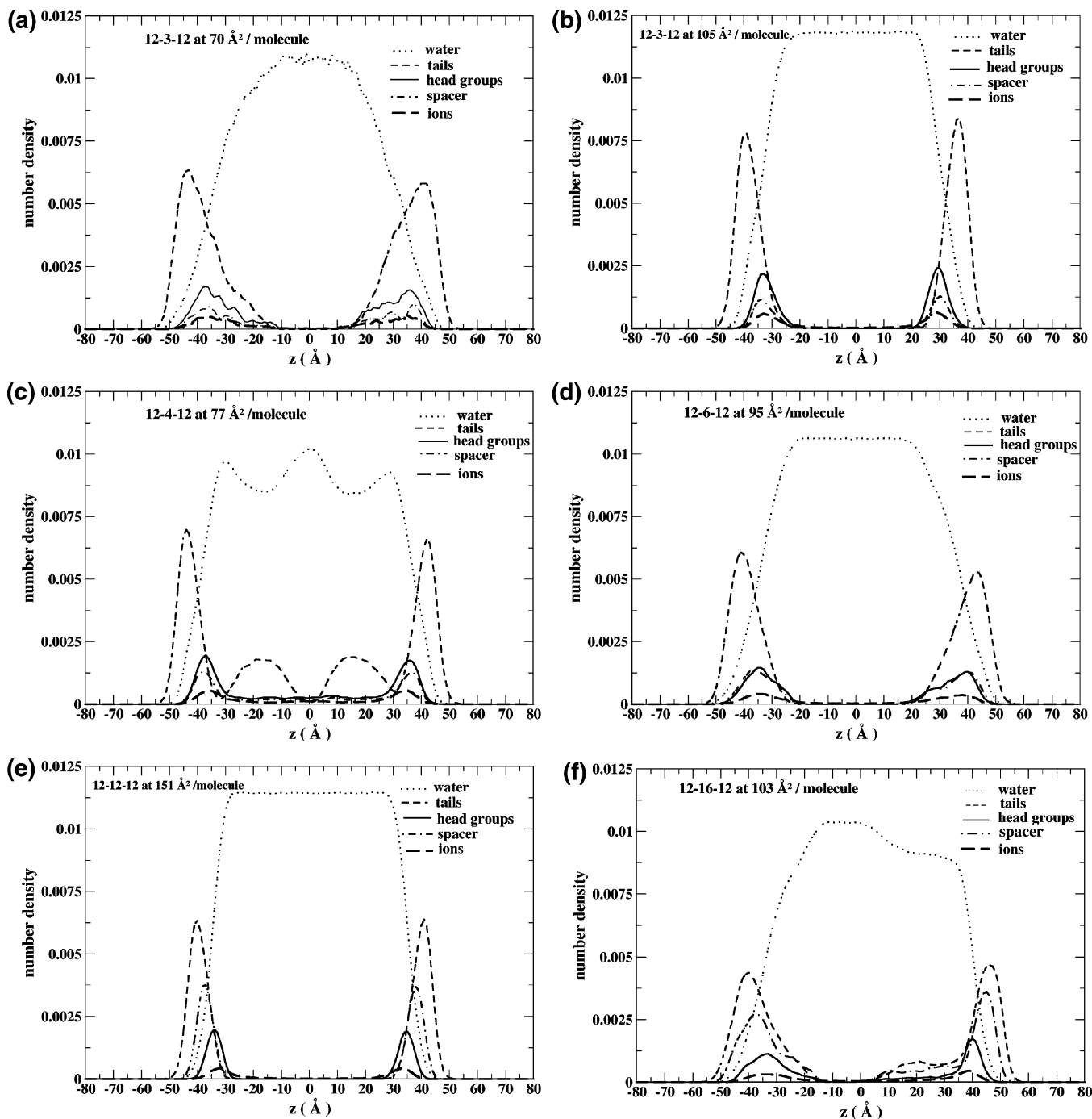


**Figure 2.** Density profiles along the  $z$  axis for the different simulation systems. The profiles for ions have been multiplied by 3 for clarity. Panels a, c, d, and f show that some surfactant molecules move below the main layer of surfactant molecules at the air/water interface. Panels b and e represent systems where an even distribution of surfactant molecules gives rise to a uniform monolayer at the air/water interface. The plots show both monolayers present at the two air/water interfaces for each system. In panels a and f, the distribution of molecules is slightly different for the two monolayers. These systems are still in the process of equilibration as discussed in the Results and Discussion section. The shape of the profiles in panels a and f could also be a result of the finite size effect arising because of the limitation of the small box size and limited number of surfactants used in the simulations.

experimentally is  $35 \text{ dynes/cm}$ .<sup>5</sup> Figure 2b shows the density profiles computed for the last 5 ns. As is clear from the figure, the surfactant molecules are well-distributed along the air/water interface, resulting in a stable monolayer. The ions are associated with the headgroups, and the spacers lie close to the headgroups. The different parameters obtained from the density profiles in Figure 2b are compared with the parameters obtained from neutron reflection experiments<sup>7</sup> in Table 2.

Figure 1b shows the average surface tension of 12-4-12 at  $A_S = 77 \text{ \AA}^2$  (system II) for the last 12 ns of the 17-ns-long simulation. As seen from the figure, the surface tension keeps

increasing with simulation time, unlike the constant surface tension curve observed for system Ib (see Figure 1a). The increase in the value of average surface tension with simulation time, as seen in Figure 1b, corresponds to movement of some surfactant molecules from the interface into the aqueous phase. The surface tension keeps changing as the number of surfactant molecules at the air/water interface changes. A constant average surface tension of the system implies a stable interface and hence a constant number of surfactant molecules at the air/water interface. After the movement of surfactant molecules from the interface into the water phase, we observe their subsequent self-

**TABLE 2: Comparison of Parameters Obtained from the MD Simulations with Those Obtained from Neutron Reflection Experiments<sup>7,a</sup>**

spacer length, $s$	conc	$\sigma_C/\text{\AA}$	$\sigma_H/\text{\AA}$	$\sigma_S/\text{\AA}$	$\sigma/\text{\AA}$ (exptl)	$\delta_{CH}/\text{\AA}$	$\delta_{CH}/\text{\AA}$ (exptl)	$\delta_{SH}/\text{\AA}$	$\delta_{SH}/\text{\AA}$ (exptl)
3	cmc/10	11.4	9.9	9.4	$13 \pm 1$	-6.4	$-5.5 \pm 1$	-0.5	NA
4	cmc	10.8	10.4	9.7	$14 \pm 1$	-6.4	$-5 \pm 1$	-0.7	$-1 \pm 3$
12	cmc	9.9	7.7	8.1	$13 \pm 1$	-5.9	$-5 \pm 1$	-3.4	$-6 \pm 3$

<sup>a</sup> Column 1 shows the length of the spacer for the surfactant 12- $s$ -12; column 2 shows the concentration corresponding to the value of  $A_S$  (for the values of  $A_S$ , see Table 1); columns 3, 4, and 5 show the full width of Gaussians at  $1/e$  of the height ( $\sigma$ ) for chains (C), headgroups (H), and spacer (S), respectively; column 6 shows the best fitted value of  $\sigma$  from neutron reflection experiments.<sup>7</sup> Columns 7 and 8 [9 and 10] show the distance between the centers of distribution of the chains [spacer] and headgroups obtained from the MD simulations and previous neutron reflection experiments, respectively. All the reported  $\sigma$  and  $\delta$  values from simulations are the averages of the values obtained for two monolayers at the two vacuum/water interfaces for each system. NA indicates that data are not available.

assembly to form spherical aggregates. This results in a well-distributed monolayer of surfactant molecules at the air/water interface, consisting of about 55 molecules, with a resultant surface area per molecule of about  $108 \text{ \AA}^2$ .

Figure 2c shows the density profiles for system II calculated over the last 2 ns. We observe two peaks for the distribution of surfactant chains for each monolayer, corresponding to aggregate formation below the primary monolayer. The density profiles obtained from our simulation are compared with the density profiles obtained from neutron reflection experiments<sup>7</sup> in Table 2. The peaks with higher number density, in the density profile of the chains, represent the primary layer. The distance between the centers of distribution of the smaller peak for hydrocarbon chains and the headgroups of the primary layer was  $19.2 \text{ \AA}$ . Li et al. observed secondary layer formation at an approximate distance of  $15\text{--}20 \text{ \AA}$  from the center of the headgroup distribution. Our simulations show that aggregate formation below the primary layer could be the reason for the observation of a secondary layer in neutron reflection experiments.

It has been observed by transmission electron microscopy that 12- $s$ -12 surfactants with a short spacer ( $s = 2$  or  $3$ ) form long, threadlike, and entangled micelles even at low concentrations, whereas they form spheroidal micelles with  $s = 4$ .<sup>27</sup> In another MD study on model water-surfactant systems, it was shown that Gemini surfactants with a spacer of two or more oil-like particles form a mixture of spheroids and tree-like micelles.<sup>28</sup> Although the above observations were for the surfactants in bulk aqueous solutions, we observe formation of spherical clusters even below the air/water interface. Figure 3a,b,c shows snapshots of the simulation at different times. At the end of the simulation, the surfactant molecules from the two initially independent monolayers are too close to each other in the form of aggregates below the interface, and the two layers start interacting with each other.

Figure 2d shows the density profiles computed for 12-6-12 at  $A_S = 95 \text{ \AA}^2$  (system III) over the last 2 ns of the simulation. We observe penetration of some surfactant molecules from the air/water interface to the aqueous phase, as seen from the density profiles. Although there is only one peak in the density profile of the chains, as compared to two peaks observed for system II (Figure 2c), the distribution is not Gaussian, as seen for system Ib (Figure 2b). The presence of one peak for the density profile of the chains for each layer makes it difficult to calculate the number of surfactant molecules in the primary layer and the molecules below it. The most direct approach to look at the structure of the layer here is to look at the snapshot of the simulation as shown in Figure 4. By looking at the snapshot, we can see that the surfactant molecules exhibit uneven distribution giving rise to a rippled surface at the air/water interface. This structure of the interface could also be a result of the initial stages of the aggregation of surfactant molecules into spherical aggregates, most likely artificially stabilized by finite size effects.

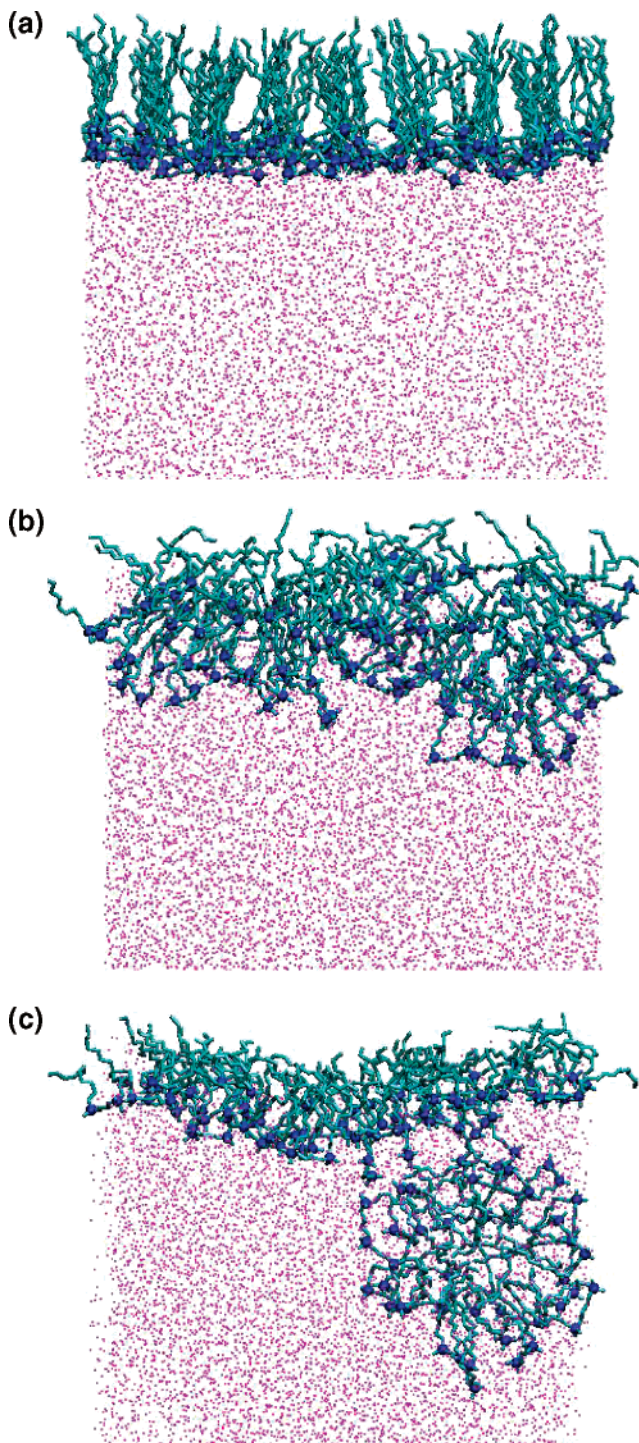
Figure 1a also shows the average surface tension of 12-12-12 at the air/water interface at  $A_S = 151 \text{ \AA}^2$  (system IV) versus simulation time, and Figure 2e shows the density profiles computed over the last 2 ns. The density profiles show the Gaussian distribution of the different fragments of the surfactant molecules. A stable monolayer with a uniform distribution of surfactant molecules exists at the air/water interface, with a constant surface tension of  $32.7 \text{ dynes/cm}$ . The structure of the stable monolayer can be seen in Figure 5, which shows a snapshot of the simulation at  $t = 10 \text{ ns}$ . Table 2 shows the various parameters obtained from the Gaussian fits to the density profiles in Figure 2e. The higher value of  $\delta_{SH}$  compared to 12-3-12 and 12-4-12 shows bending of the spacer toward hydrophobic chains in 12-12-12 as discussed above.

Figure 1a also shows the average surface tension of 12-14-12 at the air/water interface versus simulation time at  $A_S = 133 \text{ \AA}^2$  (system V). The average surface tension of the system at the end of 10 ns is  $19.2 \text{ dynes/cm}$ . We see a uniform distribution of surfactant molecules at the interface. However, we also observe large-amplitude fluctuations in the monolayer structure, and this could be the reason for a much lower surface tension value compared to that of systems Ib and IV. The density profiles obtained are very similar to system IV (Figure 2e) and are not shown here.

Figure 2f shows the density profiles computed over the last 2 ns of the simulation of 12-16-12 at the air/water interface at  $A_S = 103 \text{ \AA}^2$  (system VI). As seen from the density profiles, surfactant molecules penetrate the aqueous phase. We observe that the behavior of the system is similar to the behavior of system Ia and system II, as discussed above. We see clear aggregate formation below the air/water interface as shown in the snapshot of the system in Figure 6. We see slightly different density profiles for the two independent interfaces, as seen in Figure 2f. This could be a result of the finite size effect of using a small simulation cell, or it could be a result of the surfactant layer whose density profiles are along the negative  $z$  axis not equilibrated yet.

The high tendency of pre-micellar aggregation by Gemini surfactants has been discussed previously by many authors.<sup>3</sup> Here, we observe similar behavior for 12-3-12, 12-4-12, 12-6-12, and 12-16-12, at the air/water interface, at initial surface areas per molecule measured from surface tension measurements at the cmc. Rekvig et al. studied model linear and branched chain surfactants at the oil/water interface using dissipative particle dynamics (DPD) simulations. They also observed a curved interface and surfactant aggregation in the oil phase, at concentration below the cmc for some surfactants.<sup>29,30</sup>

Our study reveals the three-dimensional molecular structure of the secondary layer formation, supplementing the one-dimensional density profiles obtained by neutron reflectivity experiments.<sup>7</sup> However, since lowering the surface density of 12-3-12 (increasing the surface area per molecule from 70



**Figure 3.** Snapshots taken from the MD simulation of the 12-4-12 system with an initial surface area per Gemini molecule of  $77 \text{ \AA}^2$  (a)  $t = 0 \text{ ns}$ , (b)  $t = 5.5 \text{ ns}$ , (c)  $t = 17 \text{ ns}$ . Hydrocarbon chains of the surfactant molecules are rendered as green tubes, the nitrogen atoms of the headgroups as blue spheres, and the water molecules as purple points. All the hydrogen atoms and chloride ions have been removed for clarity. A spherical surfactant aggregate forms, as is clear from the last snapshot at  $t = 17 \text{ ns}$ . Only one of the two layers of surfactant molecules at the air/water interface employed in the simulation is shown for clarity. The MD simulation of the 12-3-12 system at  $70 \text{ \AA}^2$  per molecule yields similar results.

( $77 \text{ \AA}^2$  to  $105 \text{ \AA}^2$ ) results in an even distribution of surfactant molecules at the interface and no aggregate formation, the aggregation of surfactant molecules observed in these simulations could be associated with the surface area values measured experimentally. One reason for a problem could be the debatable

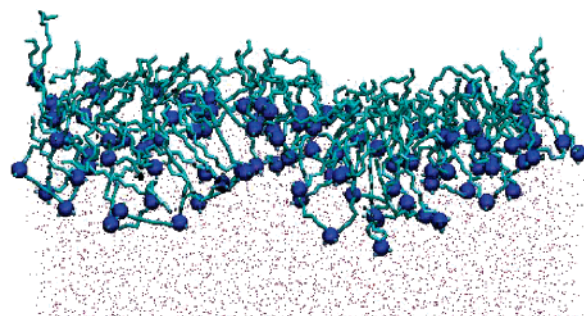


**Figure 4.** One of the monolayers from the final configuration  $t = 10 \text{ ns}$  for the 12-6-12 system at an initial surface area per molecule of  $95 \text{ \AA}^2$ . The same representation is used as described for Figure 3. An uneven distribution of molecules is seen at the air/water interface, giving rise to a rippled surface.

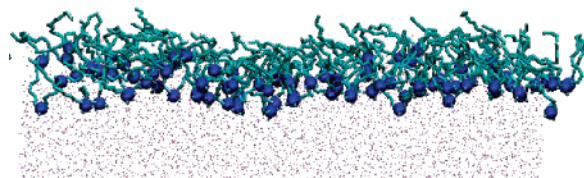


**Figure 5.** One monolayer from the 12-12-12 system at  $t = 10 \text{ ns}$  at an initial surface area per molecule of  $151 \text{ \AA}^2$ . The same representation of molecules is used as explained for Figure 3. A uniform monolayer exists throughout the simulation. Similar behavior is observed for 12-3-12 at an initial surface area per molecule of  $105 \text{ \AA}^2$  and for 12-14-12 at  $133 \text{ \AA}^2$  per molecule.

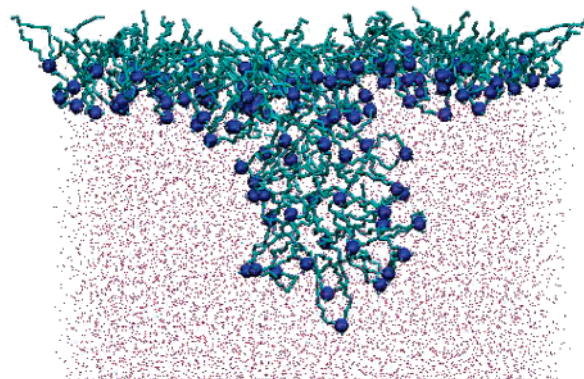


**Figure 6.** One interface taken from the simulation of the 12-16-12 system at  $t = 15 \text{ ns}$  at an initial surface area per molecule of  $103 \text{ \AA}^2$ . The same representation of molecules is used as explained for Figure 3. Surfactant is expelled from the interface and aggregate formation occurs below a monolayer of surfactant molecules at the air/water interface. The behavior of the system is very similar to that exhibited by the 12-3-12 system at  $70 \text{ \AA}^2$  per molecule and 12-4-12 at  $77 \text{ \AA}^2$  per molecule.

value of  $n$  to be used in eq 1 for calculating surface area from surface tension measurements. Although it has been argued in many papers that  $n = 2$  should be used, as discussed in the Introduction, our results here for 12-3-12 raise some doubt about the correct value of  $n$  to be used. It is clearly not easy to relate the bulk concentration of surfactants with their surface density in simulations. Rekvig et al. have combined DPD with a Monte Carlo method to determine the bulk concentration needed to obtain a given surface density of model linear and branched chain surfactants at the oil/water interface. They imposed constant surfactant chemical potential and normal pressure in separate simulations of bulk and interface.<sup>29,30</sup>

The spacer becomes more hydrophobic and flexible as the spacer length is increased. This causes bending of the spacer toward the chains, resulting in non-monotonic changes in surface

area per molecule at the air/water interface with increasing spacer length as discussed in the Introduction. Upon comparing parts a–f of Figure 2, we clearly see that the density profile of the spacer shifts toward the density profile of the chains from the density profile of the headgroups along the  $z$  axis as the number of carbon atoms in the spacer is increased. The higher value of  $\delta_{SH}$  for 12–12–12 compared to those of 12–3–12 and 12–4–12 confirms this observation. Hence, here our results agree with the previous experimental and theoretical results.

In short, the behavior of the surfactant molecules studied here can be partitioned into two general categories: In some cases, all the surfactant molecules stay at the air/water interface, giving a uniform distribution and hence a stable monolayer. In other cases, some surfactant molecules move from the air/water interface to the aqueous phase, exhibiting further aggregate formation below the interface and a stable primary monolayer at the air/water interface, with a surface concentration of the primary monolayer lower than the initial surface concentration.

## Conclusions

The behavior of the 12– $s$ –12 series of Gemini surfactants at the air/water interface has been studied by fully atomistic MD simulations using the CHARMM force field. The surfactants with  $s = 3, 4, 6, 12, 14,$  and  $16$  were studied at initial surface area per surfactant  $A_S = 70 \text{ \AA}^2, 77 \text{ \AA}^2, 95 \text{ \AA}^2, 151 \text{ \AA}^2, 133 \text{ \AA}^2,$  and  $103 \text{ \AA}^2$ , respectively. These are the surface area values derived from surface tension experiments using  $n = 2$  in the Gibbs equation at cmc. The system 12–3–12 was also studied at  $A_S = 105 \text{ \AA}^2$ . This is the surface area per molecule calculated using  $n = 3$  in the Gibbs equation. Coincidentally, this  $A_S$  value for 12–3–12 is the same as that measured at 1/10th of cmc, by neutron reflection experiments. The behavior of the surfactants was seen to depend on the values of  $s$  and  $A_S$ . Three systems studied, 12–3–12 at 1/10th of cmc (system Ib), 12–12–12 at cmc (system IV), and 12–14–12 at cmc (system V), give a continuous distribution of surfactants at the air/water interface, resulting in a stable monolayer. However, in all other situations, we observe movement of some surfactant molecules from the air/water interface into the aqueous phase. For 12–3–12, 12–4–12, and 12–16–12, we see clear formation of aggregates below the primary layer of surfactant molecules at the air/water interface. For 12–6–12, we do not see clear aggregate formation below the interface, but an uneven distribution of surfactant molecules at the interface resulting in a rippled surface exists. Our simulations provide a plausible three-dimensional molecular explanation to the observation of a secondary peak of surfactant molecules, below the primary monolayer, observed in the density profiles obtained from neutron reflection experiments. We observe the bending of the spacer toward the hydrophobic chains, as the spacer length is increased from three carbon atoms to sixteen carbon atoms. The simulations suggest that the presence of a spacer between the headgroups leads to complex behavior of the surfactants at the

air/water interface. We suggest that simulations of each surfactant molecule at different  $A_S$  values at the air/water interface, for constant  $s$ , will aid further understanding of the structure of the layers at the air/water interface at different surfactant concentrations.

**Acknowledgment.** This manuscript is dedicated to Chuck Knobler on the occasion of his 70th birthday. The authors thank Professor Robert K. Thomas for helpful discussions and the NSF and NIH for funding the research.

## References and Notes

- (1) Kern, F.; Lequeux, F.; Zana, R.; Candau, S. J. *Langmuir* **1994**, *10*, 1714.
- (2) Schmitt, V.; Schosseler, F.; Lequeux, F. *Europhys. Lett.* **1995**, *30*, 31.
- (3) Zana, R. *Adv. Colloid Interface Sci.* **2002**, *97*, 205.
- (4) Zana, R.; Benraou, M.; Rueff, R. *Langmuir* **1991**, *7*, 1072.
- (5) Alami, E.; Beinert, G.; Marie, P.; Zana, R. *Langmuir* **1993**, *9*, 1465.
- (6) Li, Z. X.; Dong, C. C.; Thomas, R. K. *Langmuir* **1999**, *15*, 4392.
- (7) Li, Z. X.; Dong, C. C.; Wang, J. B.; Thomas, R. K. *Langmuir* **2002**, *18*, 6614.
- (8) *Gemini Surfactants: Interfacial and Solution-Phase Behavior*; Zana, R., Xia, J., Eds.; Marcel Dekker Ltd.: New York, 2003; Vol. 117.
- (9) Zana, R. *J. Colloid Interface Sci.* **2002**, *248*, 203.
- (10) Diamant, H.; Andelman, D. *Langmuir* **1994**, *10*, 2910.
- (11) Diamant, H.; Andelman, D. *Langmuir* **1995**, *11*, 3605.
- (12) Maiti, P. K.; Chowdhury, D. *Europhys. Lett.* **1998**, *41*, 183.
- (13) Devinsky, F.; Lacko, I.; Bittererova, F.; Tomeckova, L. *J. Colloid Interface Sci.* **1986**, *114*, 314.
- (14) Devinsky, F.; Masarova, L.; Lacko, I. *J. Colloid Interface Sci.* **1985**, *105*, 235.
- (15) Bocker, J.; Schlenkrich, M.; Bopp, P.; Brickmann, J. *J. Phys. Chem.* **1992**, *96*, 9915.
- (16) Lee, C. Y.; McCammon, J. A.; Rossky, P. J. *J. Chem. Phys.* **1984**, *80*, 4448.
- (17) Bandyopadhyay, S.; Shelley, J. C.; Tarek, M.; Moore, P.; Klein, M. L. *J. Phys. Chem. B* **1998**, *102*, 6318.
- (18) Hautman, J.; Klein, M. L. *Mol. Phys.* **1992**, *75*, 379.
- (19) Darden, T.; York, D.; Pederson, L. *J. Chem. Phys.* **1993**, *98*, 10089.
- (20) Essmann, U.; Perera, L.; Berkowitz, M. L.; Darden, T.; Lee, H.; Pederson, L. G. *J. Chem. Phys.* **1995**, *103*, 8577.
- (21) Jorgensen, W. L.; Chandrasekhar, J.; Madura, J. D.; Impey, R. W.; Klein, M. L. *J. Chem. Phys.* **1983**, *79*, 926.
- (22) Kale, L.; Skeel, R.; Bhandarkar, M.; Brunner, R.; Gursoy, A.; Krawetz, N.; Phillips, J.; Shinozaki, A.; Varadarajan, K.; Schulten, K. *J. Comput. Phys.* **1999**, *151*, 283.
- (23) MacKerell, A. D.; Bashford, D., Jr.; Bellott, M.; Dunbrack, R. L.; Evanseck, J. D., Jr.; Field, M. J.; Fischer, S.; Gao, J.; Guo, H.; Ha, S.; Joseph-McCarthy, D.; Kuchnir, L.; Kuczera, K.; Lau, F. T. K.; Mattos, C.; Michnick, S.; Ngo, T.; Nguyen, D. T.; Prodhom, B.; Reiher, W. E.; Roux, B., III; Schlenkrich, M.; Smith, J. C.; Stote, R.; Straub, J.; Watanabe, M.; Wiórkiewicz-Kuczera, J.; Yin, D.; Karplus, M. *J. Phys. Chem. B* **1998**, *102*, 3586.
- (24) Ryckaert, J. P.; Ciccotti, G.; Berendsen, H. J. C. *J. Comput. Phys.* **1977**, *23*, 327.
- (25) Andersen, H. C. *J. Comput. Phys.* **1983**, *52*, 24.
- (26) Feller, S. E.; Pastor, R. W.; Rojnuckarin, A.; Bogusz, S.; Brooks, B. R. *J. Phys. Chem.* **1996**, *100*, 17011.
- (27) Zana, R.; Talmon, Y. *Nature* **1993**, *362*, 228.
- (28) Karaborni, S.; Esselink, K.; Hilbers, P. A. J.; Smit, B.; Karthaus, J.; van Os, N. M.; Zana, R. *Science* **1994**, *266*, 254.
- (29) Rekvig, L.; Kranenburg, M.; Hafskjold, B.; Smit, B. *Europhys. Lett.* **2003**, *63*, 902.
- (30) Rekvig, L.; Kranenburg, M.; Vreede, J.; Hafskjold, B.; Smit, B. *Langmuir* **2003**, *19*, 8195.